Depth Ranging Performance Evaluation and Improvement for RGB-D Cameras on Field-Based High-Throughput Phenotyping Robots*

Zhengqiang Fan, Na Sun, Quan Qiu*, and Chunjiang Zhao

***Abstract*— RGB-D cameras have been successfully used for indoor High-ThroughpuT Phenotyping (HTTP). However, their capability and feasibility for in-field HTTP still need to be evaluated, due to the noise and disturbances generated by unstable illumination, specular reflection, and diffuse reflection, etc. To solve these problems, we evaluated the depth-ranging performances of two consumer-level RGB-D cameras (RealSense D435i and Kinect V2) under in-field HTTP scenarios, and proposed a strategy to compensate the depth measurement error. For performance evaluation, we focused on determining their optimal ranging areas for different crop organs. Based on the evaluation results, we proposed a brightness-and-distance-based Support Vector Regression Strategy, to compensate the ranging error. Furthermore, we analyzed the depth filling rate of two RGB-D cameras under different lighting intensities. Experimental results showed that: 1) For RealSense D435i, its effective ranging area is [0.160, 1.400] m, and in-field filling rate is approximately 90%. 2) For Kinect V2, it has a high ranging accuracy in the [0.497, 1.200] m, but its in-field filling rate is less than 24.9%. 3) Our error compensation model can effectively reduce the influences of lighting intensity and target distance. The maximum MSE and minimum R^2 of this model are 0.029 and 0.867, respectively. To sum up, RealSense D435i has better ranging performances than Kinect V2 on in-field HTTP.**

I. INTRODUCTION

As a typical application of agricultural robots, field-based HTTP robots have been an important research topic of plant phenomics[1, 2]. They are widely used to extract the morphological/physiological parameters of crops on a large scale[3]. In crop breeding, the mass sample screening highly relies on manual screening, which is a time consuming, laborious, high cost and low-throughput style[4]. For breaking this bottleneck, researchers try to use robots to replace human beings, which can achieve high-throughput, high-precision and low-cost screening of crop samples in an automated manner[5, 6]. This is a significant work for improving breeding efficiency and increasing crop yields[7].

HTTP robots consist of three components: phenotyping platforms, sensors and parameter extraction algorithms of crop traits[8]. Phenotyping platforms equipped with different types of sensors are used to collect 2D/3D information of crops. Intelligent algorithms extract crop parameters of interest to breeders, which can be used to guide breeding research[9]. Among common sensors for HTTP robots, RGB-D cameras are drawing more and more attentions because of their low cost and informative capacities[10, 11]. They can obtain both color and depth images in the same frame at close range, which is a distinguishing advantage in organ detection and measurement of crops.

The research of HTTP robots with RGB-D cameras has made successful achievements for indoor applications. However, in-field scenes are quite different from indoor scenes. As the main cultivation mode of crops, field planting is easy to be disturbed by external factors (e.g. illumination) and not controllable[12]. As a result, indoor phenotyping technologies, such as RGB-D data, can't be directly transferred to outdoor cases. It is necessary to develop outdoor and in-field RGB-D data analysis solutions for HTTP robots. In this paper, we evaluate the performances of consumer-level RGB-D cameras and propose a novel method to improve their in-field measurement accuracy.

The main contribution of this paper is providing a solution to decreasing the effects of illumination and distance on RGB-D cameras under in-field scenarios. We first determine the optimal ranging areas and the depth measurement accuracy for different crop organs under different lighting intensities. This provides an intuitive evaluation of ranging performances and quantifies the effects of illumination and distance. Second, we propose a novel strategy to compensate the depth measurement error. Third, we calculate the filling rate of depth images under different lighting situations. After correlation analysis of effective ranging area and in-field filling rate, we can get an intuitive accuracy ranking diagram.

II. RELATED WORK

To improve the in-field performances of RGB-D cameras, a lot of efforts have been made. In particular, the effect of light changes on measurements has been widely concerned. There are two ways to solve this problem: 1) controlling the interference from external light sources; 2) evaluating the sensor performances under different external environments.

A. Light Source Control

Researchers try to cut down the influence of illumination changing with three ways during the data collection process: 1) Shading or light supplementing. Gongal et al.[13] used a

*Resrach supported by National Key Research and Development Program of China (No. 2017YFD0700303), and National Natural Science Foundation of China (No.61973040).

Zhengqiang Fan and Na Sun are with Beijing Research Center of Intelligent Equipment for Agriculture, Beijing Academy of Agriculture and Forestry Sciences, Beijing, 100097 China.

Quan Qiu is with Beijing Research Center of Intelligent Equipment for Agriculture, Beijing Academy of Agriculture and Forestry Sciences, Beijing, 100097 China. (+86 18610049569; e-mail: qiuq@nercita.org.cn, 179640136@qq.com).

Chunjiang Zhao is with Beijing Research Center for Information Technology in Agriculture, Beijing Academy of Agriculture and Forestry Sciences, Beijing, 100097 China.

PMD CamCube 3D camera and other sensors to identify apples in the orchard. To reduce the variability of lighting conditions, they employed an opaque tarpaulin to block the light, and LED lights to maintain stable lighting conditions. 2) Conducting the data collection at night or on a cloudy day. Bao et al.[14] obtained the 3D morphological structures of maize crops with an RGB-D camera carried by a mobile platform at night. 3) Post-processing. RGB-D images obtained in-field were post-processed to improve the accuracy of phenotypic data. Milella et al.[15] applied color enhancement and deep learning to estimate the volume and quantity of the grape clusters in the vineyard based on data collected with RGB-D cameras.

It is an effective method to improve the performance of RGB-D cameras by controlling the light sources. But, it's not the best way to extract crop phenotypic parameters. It is well known that the growth cycle of crops is short, we must obtain more phenotypic data in the shortest time. However, controlling the light sources requires more time to deploy hardware resources and software algorithms. Conducting data collection at night seriously reduces the working efficiency.

B. Ranging Performance Evaluation

In order to quantify the outdoor performances of RGB-D cameras, researchers evaluated them from the perspective view of sensor intrinsic parameters. Piatti et al.[16] assessed the influences of warm-up and integration time on distance measurements for two Time-of-Flight (ToF) cameras, SR-4000 and CamCube3.0. Kazmi et al.[17] compared the different performances of three ToF cameras (CamBoard, CamCube and SR4000) on leaves depth imaging with stereo vision sensors under different lighting conditions, and proposed a method to improve the application performances of sensors under different shadow and sunlight exposure scenes. He et al.[18] analyzed the influences of typical external distractions including material, color, distance and lighting on the depth error of ToF cameras. At the same time, an error correction method was proposed based on Particle Filter and Support Vector Machine (PFSVM). Vit et al.[19] compared the filling rate of the in-field crop depth images from four common RGB-D cameras (ORBBEC Astra S, Microsoft Kinect V2, Intel RealSense SR300 and Intel RealSense D435).

Although there have been many assessments of RGB-D camera performances for outdoor applications, it is still an open question to evaluating the 3D plant morphological data collection under natural lighting situations. There are various factors influencing the data collection performances of RGB-D cameras, including the heavily changing lighting conditions during the day time and the different reflection characteristics of different organ parts.

III. METHODS

The ranging performances of RGB-D cameras have been evaluated in some regular scenes. Although different factors (i.e. color, temperature, texture, shape) need different evaluation operations, the evaluations processes share certain common parts, such as variable control, data acquisition, data analysis and accuracy Ranking. Unfortunately, external perturbation factors cannot be controlled, when RGB-D cameras are applied for in-field measurement. Therefore, conventional evaluation methods can't meet the need of depth performance evaluation for RBG-D camera based in-field phenotyping. As a result, we propose a novel ranging assessment and error compensation strategy by adding two new skills into the operation process:

- *Central-Region-Based Depth-Ranging Evaluation:* It is an impossible mission to evaluate the depth values one by one in a depth image. Thus, we assume that the central region pixels of a depth image enjoy the best or above average depth accuracy among the whole pixel-depth set. Then, we just need to evaluate the optimal ranging areas and measuring accuracy using the central region. To be noted, we evaluate the ranging performances for different crop organ parts.
- *Error Compensation:* To improve the depth ranging accuracy, we propose a new error compensation strategy based on SVR, which employs image brightness and distance as inputs. The strategy can effectively reduce the negative effects caused by lighting intensity and distance.

A. Determining the Depth Value for the Central Region

For an image with *r* rows and *c* columns of pixels, the central pixel is unique only if *r* and *c* are both odd numbers. Unfortunately, *r* and *c* are both even numbers in most cases, including the two RGB-D camera cases in this paper. At the same time, a central pixel has high probability to be invalid depth value. So we choose the effective mean depth value of the central region (*h* height and *w* width) as the central point depth for a single frame. In addition, the depth value of each frame is easy to fluctuate slightly. Therefore, for each central region, we capture *m* frames of depth images, and compute the mean value of the all frames as the final central depth value. The depth value of the center region is calculated as following:

$$d = \frac{\sum_{f=1}^{m} \overline{d}_{center\_h \times w}^{(f)}}{m} \tag{1}$$

here, $\overline{d}_{center\_h \times w}^{(f)}$ is the effective mean depth value of *h* height and *w* width from the center region for a single-frame depth image. *m* represents the number of frames of the acquired depth images. *d* is the final measurement value from the mean value of *m* depth frames. We take this value as an index to evaluate the ranging performances of RGB-D cameras.

B. SVR Based Error Compensation Model

Lighting intensity and target distance are the main factors which affect the measurement accuracy of RGB-D cameras. The effects of lighting intensity are more difficult to handle than those of target distance. Because we can't get lighting intensity in real-time during experiments. To tackle this problem, we propose an SVR based error compensation strategy. This strategy can reduce the effects of lighting

intensity and target distance on the depth measurement accuracy.

This strategy includes two key steps: 1) Finding the functional relationships of lighting intensity and brightness, so as to use brightness to compensate the measurement error caused by lighting intensity. The brightness of the measuring target can be obtained from the color image of the RGB-D camera. Here, we extract the brightness value by converting the image from RGB space to HSV space. 2) Employing SVR to build error compensation model. Based on the multi-input characteristics of SVR, we take target distance and the brightness as inputs, and the error compensation results as the output, to improve the measurement accuracy.

The relationship of lighting intensity and brightness should fit the following constraints: 1) the function must pass through zero; 2) as lighting intensity approaches infinity, brightness approaches one. In addition, it is suggested that the color information of the image is as monotonous as possible, to better fit the regression model of lighting intensity and brightness. Applying nonlinear function regression on the brightnesses of green plant images under different lighting intensities, the following function can be obtained:

$$y = 1 - \frac{1}{ax^b + 1} \tag{2}$$

where, a=0.9313, b=0.0682. The terms x and y represent the lighting intensity and brightness, respectively.

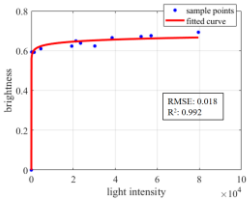

Figure 1. Regression curve of light intensity and brightness

Fig.1 shows their relationship curve. We can use image brightness other than lighting intensity to compensate ranging errors, which avoids obtaining lighting intensity in real-time.

Brightness-and-distance-based SVR is a multi-input black-box model for nonlinear systems[20]. Here we take the brightness and the measured values as input, the measuring deviation values as output, and adopt the SVR based on the Gaussian kernel function to establish the deviation model. In this model, we employ grid search based on K-fold cross-validation (K-CV) to determine the optimal penalty factor C and Gaussian kernel parameter G[21]. In the experiment of error compensation, we collect 100 sets of data samples. These data contain two eigenvectors and a label. The eigenvectors are measured values and brightness values. The label is measured deviations, which can be calculated by:

$$D = L_m - L_b \tag{3}$$

where, D is measured deviation, L_m and L_b are measured value and benchmark value, respectively. In fact, these datasets usually have some outliers due to external disturbances. Thus, we first need to preprocess the datasets. We define outliers as data values with the differences of the measured deviations and the means, which is at least three times bigger than the standard deviation from label datasets. The formula for detecting outliers can be expressed as:

$$\begin{aligned} &V_{\text{outlier}} = D - D_m - 3D_s \\ &s.t. \quad D - D_m - 3D_s \geq 0 \end{aligned} \tag{4}$$

where, D, D_m, and D_s are measured deviation, means and standard deviation, respectively. For keeping the sample size, we replace the outliers with the nearest non-outlier elements. Then, we divide the datasets into training sets and test sets in a 2:1 scale. Because our purpose is to reduce the measured deviation caused by the target distance and light intensity, we need to convert the brightness to light intensity with function (2). Thus, the light intensity can be indirectly obtained by brightness. As a result, the two eigenvectors from datasets are measured values and light intensities. Generally, the range of value domains for two eigenvectors differs greatly, so we need to normalize the datasets. The formula of normalization is:

$$y = (y_{\max} - y_{\min}) \times \frac{x - x_{\min}}{x_{\max} - x_{\min}} + y_{\min} \tag{5}$$

where, x is training sets or testing sets, y is normalization results. $y_{\min}$ and $y_{\max}$ carry out the normalized numerical interval. We set them as -1 and 1, respectively. Next, we select SVR model parameters, which consists of the optimal penalty factor C and Gaussian kernel parameter G. Grid search algorithms based on K-CV includes four steps to find the optimal parameters.

- *Establishing Grid Coordinates:* The range of parameter optimization is determined by grids. To ensure a wide enough parameter searching range, we use exponential function to divide the grid. We suppose the grid coordinates are a and b,

$$\begin{aligned} a &= [-m, m] \\ b &= [-n, n] \end{aligned} \tag{6}$$

here, m and n are the range of plane coordinates. Thus, the range of model parameters is:

$$\begin{aligned} c &= \left[-u^m, u^m\right] \\ g &= \left[-v^n, v^n\right] \end{aligned} \tag{7}$$

here, u and v are the base of exponential functions, which can be randomly chosen according to practical requirements.

- *Dividing the Sample with K-CV:* We divide the training set into K subsets, and use these subsets for K times cross-validation.
- *Determining Prediction Error:* We take the mean square error of K test results in the previous step as the performance index of the model.
- *Determining the Optimal Combination Parameters:* We take c and g corresponding to the minimum mean square error as the optimal parameters.

Finally, we can build the error compensation model by substituting C and G into SVR. To better demonstrate the effect, we can reverse normalize the predicted results.

C. Filling Rate Calculation for Crop Regions

After the ranging performance is evaluated, we need know

the filling rate of the depth images. The traditional statistic method of filling rate calculation is for the whole image. Here, we only concern the crop regions, not the whole image. As a result, we propose a method to calculate the crop region filling rate. Our approach is divided into four steps:

- *Extracting Crop Pixels:* We extract the R \ G \ B color pipelines from the obtained color images, and employ grayscale method based on the extra green (*ExG*) index to enhance the crops information of image pixels[22]. The expression of *ExG* is:

$$ExG = 2G - R - B \tag{8}$$

- *Obtaining Binary Grayscale Image:* We employ the automatic threshold segmentation method based on Ostu to obtaining the binary grayscale image and then segment the crop and background information.

- *Mask Processing:* We traverse all pixels in the binary image, replace the 0s with "NaN" and the 255s with the corresponding depth value from depth images.

- *Calculating Filling Rate:* We count the number of zeros and nonzeros in the masked images. It should be noted that "NaN" is not within the statistical scope. As a result, filling rate can be calculated by formula:

$$F = \frac{M - N}{M} \tag{9}$$

where, *F* is the filling rate, *N* is the number of 0s, and *M* is the number of pixels replaced by the depth value.

IV. Experimental Results

A. Experimental Settings

In our experimental platform, field phenotypic data were collected by a portable mobile workstation equipped with two consumer-level depth cameras, Intel® RealSense D435i (RS D435i) and Microsoft® Kinect V2 (Kinect V2). Their working principles for color and depth information collection are infrared active stereoscopy and Time-of-Flight technology, respectively. To evaluate the depth accuracy, a hand-held single-point laser rangefinder was employed to obtain the depth benchmark values, whose resolution is ± 1mm. The light intensity was measured by a LI-COR Li-250A light meter, whose resolution is ±10 lux. To collect measurement values for different organs of crops, all the sensors were placed on a mobile platform. The algorithms we developed are coded under Robot Operating System based on Ubuntu 16.04.

We carried out experiments in three scenes: different day time, different weather, and different surface reflection quantities. Maize is a typical kind of grain and cash crop. We chose its three organs (stalk, leaf and maize cob) as the typical measuring targets. To evaluate the depth ranging performances, we focused on the analysis of the three main factors which introduce in ranging error. These factors include lighting intensity, incident angle of light, and surface reflection of the crop organs. Specifically, the first two factors are analyzed in SEC. IV-B. We collected ranging data at different day time (different lighting intensities and incident angles), under both cloudy and sunny weather conditions (different lighting intensities). The different surface reflection quantities are analyzed in SEC. IV-C. We collected ranging data on different organ surface parts. For the leaf surface, we further categorized the surfaces into three subgroups: the front surface, the rear surface, and the tip. The front and the rear surfaces are two sides of the leaf. Here, we take the leaf side facing the sun as the front surface, and take the other side as the rear surface. The tip accounts for about one tenth of a leaf surface. The accurate detection of the leaf tip is important to the crop 3D reconstruction and the extraction of crop phenotyping parameters. In addition, the error compensation result is discussed in SEC. IV-D, and the filling rate of crop pixels for different scenes is analyzed in SEC. IV-E.

For all above cases, we tested the influences coming from different pixel resolutions. For Kinect V2, we chose only one resolution (512 x 424). While for RS D435i, we chose three resolutions: 640 x 480, 848 x 480 and 1280 x 720. The data acquisition frequency was 30fps for all resolutions.

B. Optimal Ranging Areas

Maize stalk is under the canopy, which greatly cuts down the influences from changing illumination conditions. As a result, we take the stalk as a typical object to evaluate the ranging performances. In the experiment, we set the center region of images from RGB-D cameras to be 10 x 10 pixels. For each target point, we first mark it using a single-spot laser rangefinder and obtain its corresponding benchmark depth value. Then, we capture 100 frames of depth images by deploying the RGB-D cameras at the same position and observation orientation as the laser rangefinder. Here, we can get the measurement values according to the approach of SEC. III-A. The ranging performances are analyzed by comparing the deviations between the benchmark and measurement values. Fig.2 shows the flow diagram of data collection.

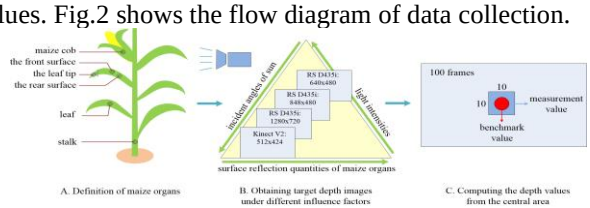

Figure 2. The flow diagram of data collection

Fig.3(A) shows the minimum ranging performances of two cameras under different lighting intensities. We can find that RS D435i has smaller fluctuations than Kinect V2 on minimum measurement distance. For RS D435i, higher resolution leads to larger minimum range. At the same time, the minimum ranging performances for the three resolutions of RS D435i are almost not influenced by the changing light intensities. However, for Kinect V2, its minimum range increases gradually with the changing light intensities. To ensure that the two cameras can obtain depth values under any in-field lighting intensities, we take the maximum value of all measured distances as the minimum range. As a result, we can infer that RS D435i's minimum ranges of three resolutions 640 x 480, 848 x 480 and 1280 x 720 are 0.160m, 0.172m and 0.262m, respectively. Kinect V2's minimum range is 0.497m.

Fig.3(B) shows the deviations of the minimum ranges and their benchmark values under different lighting intensities. We can find that all of the measurement errors are less than 0.003m. This shows that the both cameras have high depth accuracies around their minimum ranges.

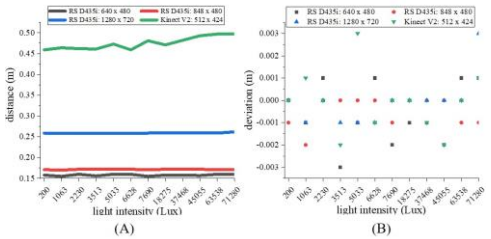

Figure 3. Minimum ranges and deviation of two cameras

The other indicator of optimal ranging areas is the maximum range. Fig.4 shows root mean square error (RMSE) for the deviations of measured and benchmark values.

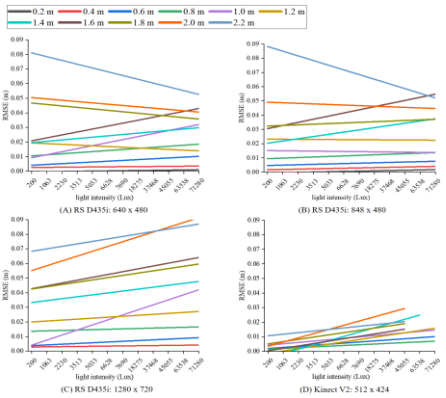

Figure 4. The RMSE of ranging deviation of two cameras for different distances with changing light intensities

Different colored curves represent the linear fitting results of RMSE at different distances. The four subgraphs represent the RMSE distribution of two cameras under different resolutions.

TABLE I. EFFECTIVE RANGING AREAS OF TWO CAMERAS

		RS D435i			Kinect V2
		640 x 480	848 x 480	1280 x 720	512 x 424
ERA	Min (m)	0.160	0.172	0.262	0.497
	Max (m)	1.4	1.4	1.2	1.2

To quantify the RMSE distributions, we take 0.03m as a threshold. For 640 x 480 and 848 x 480 of RS D435i, we can find that their RMSEs can roughly meet the threshold under different lighting conditions, when the measurement distance is within 1.4m. While for 1280 x 720, its effective ranging is 1.2m. Then we can infer that greater resolution doesn't mean better ranging performances. For Kinect V2, its RMSE curve is always under 0.03m at all test distances. However, its available range decreases with the rising of lighting intensity. Therefore, we take 1.2m as its maximum range. According to the above analysis, we can get the effective ranging areas (ERA) of two cameras as shown in Table I.

C. Measurement Accuracies for Different Maize Organs

In this part, we further focus on the measurement accuracies for other maize organs within the ERA. To evaluate the influences of organ surface reflection, we select two specific cases: first, targets lying in the shadow; second, targets directly lying under the sun. To keep the lighting conditions stable, all data are collected during the same time duration of adjacent days with similar weather conditions. When the target organs lie in the shadow, the lighting intensity of their nearby areas is around 18000 Lux; when the target organs lie under the sun, the lighting intensity of their nearby areas is around 42000 Lux.

In the experiment, we find that the RMSE of two cameras remained within a region of [0, 0.03] m, when the distance between crop organs and the cameras is less than 1m. The RMSEs of different organ parts increase rapidly when the measuring distance is greater than 1m. As a result, we evaluate the measuring accuracy of organ parts within the range of [1, 1.4] m. For each organ, we calculate the mean values of the RMSEs (M-RMSE) for lighting intensities of 18000 Lux and 42000 Lux, which are used to evaluate the measurement accuracy of each organ. For the three resolutions of RS D435i, we can see from Fig.5 that the RMSEs of 42000 Lux is greater than those of 18000 Lux. The polylines generated by M-RMSE show the measurement accuracies of each organ. The minimum M-RMSE (or the highest accuracy) comes from the case of "front of the leaves", following by the cases of "back of leaves", "tip of leaves", "maize cob". The poor detection accuracy of maize cobs may be related to the growth period of maize. The newly grown maize cobs have a smooth surface, which is prone to cause specular reflection. For Kinect V2, measuring accuracy is independent with each organ.

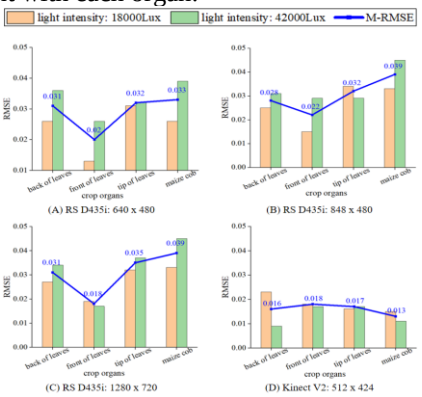

Figure 5. Measurement accuracies of two cameras for different organs

D. Depth Error Compensation

From parts A to C, we know light intensity and distance have effects on the performances of RGB-D cameras. Here, we test our brightness-and-distance-based SVR strategy for depth error compensation. In the experiment, we set both the grid coordinates u and v as 2, and use 5-fold cross-validation (K=5). Fig.6 shows the results of our strategy on the two cameras at different resolutions. Table II shows the mean square error (MSE) and R^2 correlation coefficient of our regression models. MSE and R^2 are calculated with the optimal penalty factor C and Gaussian kernel parameter G

from K-CV. We can find that the maximum MSE and minimum R^2 of error regression models are 0.029 and 0.867, respectively. The experimental results show that the novel depth error compensation strategy can effectively build the error model and improve the measuring accuracy.

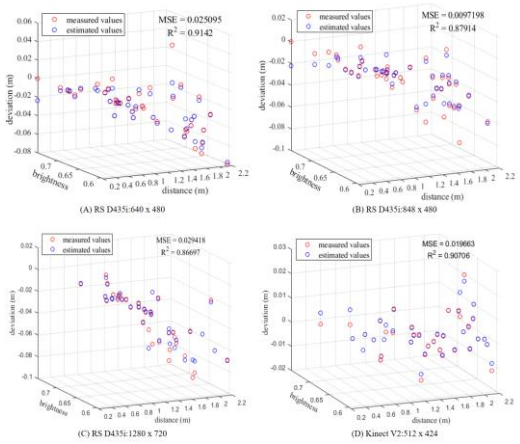

Figure 6. Error compensation results

TABLE II. CORRECTION RESULTS OF MEASURING ERROR

	RS D435i 640 x 480	RS D435i 848 x 480	RS D435i 1280 x 720	Kinect V2 512 x 424
C	2	0.3536	16	5.6569
G	256	512	181.0193	512
MSE	0.025	0.001	0.029	0.020
R^2	0.914	0.879	0.867	0.907

E. Crop Region Filling Rate

Here, we focus on the filling rate of plants in depth images. To evaluate the influences of lighting changes, we carry out experiments under three scenes: facing-to-sun (FS) in-field, back-to-sun (BS) in-field, and in greenhouse. The lighting intensities of these three scenes are 42000 Lux, 18000 Lux and 34000 Lux, respectively. Fig.7 shows the colored image and its corresponding results of extracted crop pixels using the method of SEC. III-C. Fig.7(D) shows the effect of replacing crop pixels in the binary image with depth values.

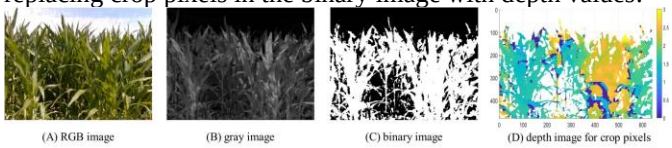

Figure 7. Measurement accuracies of two cameras for different organs

Fig.8 shows the filling rates of two cameras under different application scenes. In Fig.8, RS D435i has better filling rates than Kinect V2. All three resolutions of RS D435i enjoy high crop region filling rate above 90%, which indicates that illumination has little influence on RS D435i's filling rate. The filling rate is lower in greenhouse and BS cases, possibly due to specular reflections from some crop organs. For Kinect V2, the higher the outdoor lighting intensity is, the lower the filling rate is, which indicates that its filling rate is greatly affected by the lighting intensity. Especially under strong light outside, the filling rate is almost 0. Kinect V2's largest filling rate of 66.21% appears in the greenhouse. The results verify that Kinect V2 has poor ranging filling rate under strong light and is not suggested for outdoor applications.

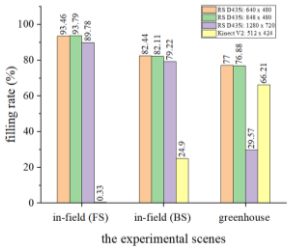

Figure 8. Filling rates of two cameras under different application scenes

Based on the correlation analysis of effective ranging area and in-field filling rate of two RGB-D cameras, we can get an intuitive accuracy ranking diagram, as shown in Fig.9. Here, for RS D435i, we set up a transition area [1.2, 1.4] m. Because the resolution 1280 x 720 of RS D435i has a maximum measurement distance of 1.2m. It should be noted that unstable area indicates a lower filling rate.

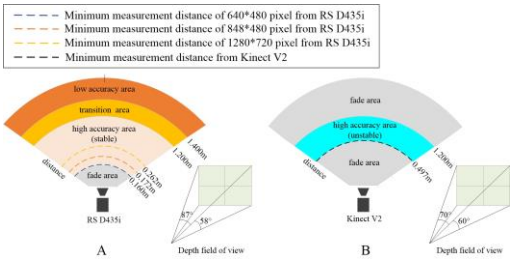

Figure 9. Accuracy ranking diagram

V. DISCUSSION AND CONCLUSION

We evaluate the depth ranging performances of two RGB-D cameras (RS D435i and Kinect V2) on HTTP robots, and propose a novel error compensation strategy. According to the experimental results, we can infer that RealSense D435i has better performances for in-field high-throughput crop phenotyping than those of Kinect V2.

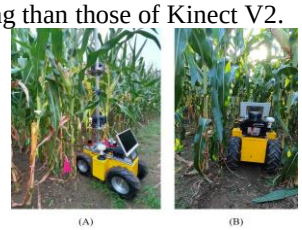

Figure 10. PhenoBotist

This work is of great significance for in-field HTTP. The effective measurement range of RGB-D cameras can guide the users to deploy the sensors at the optimal position on the phenotyping platform, which makes the images collected by RGB-D cameras more available. The measuring accuracy of each organ and the filling rate of crops play an important role in the process of 3D crop model reconstruction. The proposed SVR can greatly improve the measurement accuracy of RGB-D cameras. Now, we are developing an in-field phenotyping robot-PhenoBotist, which can move in maize row and conduct on-line HTTP.

REFERENCES

[1] N. Chebrolu, P. Lottes, A. Schaefer, W. Winterhalter, W. Burgard, and C. Stachniss, "Agricultural robot dataset for plant classification, localization and mapping on sugar beet fields," *The International Journal of Robotics Research*, vol. 36, no. 10, pp. 1045-1052, 2017.

[2] D. Ball, B. Upcroft, E. van Henten, A. van den Hengel, P. Tokekar, and J. Das, "JFR Special Issue on Agricultural Robotics," *Journal of Field Robotics*, vol. 34, no. 6, pp. 1037-1038, 2017.

[3] P. Kurtser, O. Ringdahl, N. Rotstein, R. Berenstein, and Y. Edan, "In-Field Grape Cluster Size Assessment for Vine Yield Estimation Using a Mobile Robot and a Consumer Level RGB-D Camera," *IEEE Robotics and Automation Letters*, vol. 5, no. 2, pp. 2031-2038, 2020.

[4] W. Yang *et al.*, "Crop Phenomics and High-Throughput Phenotyping: Past Decades, Current Challenges, and Future Perspectives," *Molecular Plant*, vol. 13, no. 2, pp. 187-214, Feb 3 2020.

[5] Z. Zhang, E. Kayacan, B. Thompson, and G. Chowdhary, "High precision control and deep learning-based corn stand counting algorithms for agricultural robot," *Autonomous Robots*, vol. 44, no. 7, pp. 1289-1302, 2020.

[6] S. N. Young, E. Kayacan, and J. M. Peschel, "Design and field evaluation of a ground robot for high-throughput phenotyping of energy sorghum," *Precision Agriculture*, vol. 20, no. 4, pp. 697-722, 2018.

[7] J. Bailey-Serres, J. E. Parker, E. A. Ainsworth, G. E. D. Oldroyd, and J. I. Schroeder, "Genetic strategies for improving crop yields," *Nature*, vol. 575, no. 7781, pp. 109-118, Nov 2019.

[8] C. Zhao *et al.*, "Crop Phenomics: Current Status and Perspectives," *Frontiers in Plant Science*, vol. 10, p. 714, 2019.

[9] T. Mueller-Sim, M. Jenkins, J. Abel, and G. Kantor, "The Robotanist: a ground-based agricultural robot for high-throughput crop phenotyping," in *2017 IEEE International Conference on Robotics and Automation (ICRA)*, 2017, pp. 3634-3639: IEEE.

[10] J. R. Rosell-Polo *et al.*, "Kinect v2 Sensor-Based Mobile Terrestrial Laser Scanner for Agricultural Outdoor Applications," *IEEE/ASME Transactions on Mechatronics*, vol. 22, no. 6, pp. 2420-2427, 2017.

[11] A. Durand-Petiteville, E. Le Flecher, V. Cadenat, T. Sentenac, and S. Vougioukas, "Tree Detection with Low-Cost Three-Dimensional Sensors for Autonomous Navigation in Orchards," *IEEE Robotics and Automation Letters*, vol. 3, no. 4, pp. 3876-3883, 2018.

[12] I. C. F. S. Condotta, T. M. Brown-Brandl, S. K. Pitla, J. P. Stinn, and K. O. Silva-Miranda, "Evaluation of low-cost depth cameras for agricultural applications," *Computers and Electronics in Agriculture*, vol. 173, 2020.

[13] A. Gongal, A. Silwal, S. Amatya, M. Karkee, Q. Zhang, and K. Lewis, "Apple crop-load estimation with over-the-row machine vision system," *Computers and Electronics in Agriculture*, vol. 120, pp. 26-35, 2016.

[14] Y. Bao, L. Tang, S. Srinivasan, and P. S. Schnable, "Field-based architectural traits characterisation of maize plant using time-of-flight 3D imaging," *Biosystems Engineering*, vol. 178, pp. 86-101, 2019.

[15] A. Milella, R. Marani, A. Petitti, and G. Reina, "In-field high throughput grapevine phenotyping with a consumer-grade depth camera," *Computers and Electronics in Agriculture*, vol. 156, pp. 293-306, 2019.

[16] D. Piatti and F. Rinaudo, "SR-4000 and CamCube3.0 Time of Flight (ToF) Cameras: Tests and Comparison," *Remote Sensing*, vol. 4, no. 4, pp. 1069-1089, 2012.

[17] W. Kazmi, S. Foix, G. Alenyà, and H. J. Andersen, "Indoor and outdoor depth imaging of leaves with time-of-flight and stereo vision sensors: Analysis and comparison," *ISPRS Journal of Photogrammetry and Remote Sensing*, vol. 88, pp. 128-146, 2014.

[18] Y. He, B. Liang, Y. Zou, J. He, and J. Yang, "Depth Errors Analysis and Correction for Time-of-Flight (ToF) Cameras," *Sensors (Basel)*, vol. 17, no. 1, Jan 5 2017.

[19] A. Vit and G. Shani, "Comparing RGB-D Sensors for Close Range Outdoor Agricultural Phenotyping," *Sensors (Basel)*, vol. 18, no. 12, Dec 13 2018.

[20] C. C. Chang and C. J. Lin, "LIBSVM: A Library for Support Vector Machines," (in English), *Acm Transactions on Intelligent Systems and Technology*, Article vol. 2, no. 3, p. 27, 2011, Art. no. 27.

[21] L. Yao, Z. Fang, Y. Xiao, J. Hou, and Z. Fu, "An Intelligent Fault Diagnosis Method for Lithium Battery Systems Based on Grid Search Support Vector Machine," *Energy*, vol. 214, 2021.

[22] H. Liu, H. Sun, M. Li, and M. Iida, "Application of Color Featuring and Deep Learning in Maize Plant Detection," *Remote Sensing*, vol. 12, no. 14, 2020.